Journal of Magnetic Resonance 309 (2019) 106626

Contents lists available at ScienceDirect

Journal of Magnetic Resonance

journal homepage: www.elsevier.com/locate/jmr

Application of copper plates for frequency tuning of surface wired and wireless MRI coils

Mikhail V. Gulyaev [a,*], Olga S. Pavlova [a], Dmitry V. Volkov [a], Elnur G. Sadykhov [b], Nikolay V. Anisimov [a], Yury A. Pirogov [a,b]

[a] Lomonosov Moscow State University, Moscow 119991, Russia
[b] National Research Nuclear University "MEPhI", Moscow 115409, Russia

ARTICLE INFO

Article history:
Received 2 August 2019
Revised 14 October 2019
Accepted 23 October 2019
Available online 24 October 2019

Keywords:
Frequency tuning
Surface coil
Copper plate
Radiofrequency shielding
Multinuclear magnetic resonance
Multi-turn multi-gap transmission line resonator

ABSTRACT

This study shows how a copper plate could be used for frequency tuning of surface wired and wireless MRI coils. For this purpose, it is proposed to place the copper plate directly on their conducting circuit. This leads to increase in the resonance frequency of coils. The effect is most perceptible if the copper plate is comparable in size to the conducting circuit of radiofrequency (RF) coil. The experimental work was performed on a 7.05 T MR scanner using surface MRI coils operating on different resonance frequencies: ^{1}H (300 MHz), ^{31}P (121 MHz), ^{23}Na (79 MHz), ^{13}C (75 MHz). Application of copper plate for frequency tuning of wireless multi-turn multi-gap transmission line resonator (MTMG-TLR) was considered for the first time. The proposed method can be claimed if the nominal variable inductance or capacitance is not enough for tuning the resonance frequency of the MRI coil to a higher frequency range.

1. Introduction

Tuning radiofrequency (RF) coil to a certain resonance (Larmor) frequency is a necessary step in magnetic resonance imaging (MRI) and spectroscopy (MRS) [1,2]. Typically, this procedure is carried out using variable tuning capacitors and/or inductances, included in the electric circuit of the coil, as well as using varactor diodes [3,4]. Based on this standard tuning method, a large number of RF coils have been developed, which can adapt to different objects of study and operate in different frequency ranges. In practice, however, we have to deal with a limited set of coils, the characteristics of which may not fully correspond to a specific area of study. If the purchase or manufacture of the suitable coil cannot be made, it is important to be able to find a simple technical solution and the available resources to tune the frequency of an existing coil to the desired resonance frequency.

It is known from electrodynamics that when a conductive material is placed near the oscillatory RLC circuit or RF coil, the effect of mutual inductance is observed [5]. As a result, the effective inductance of RF coil decreases, which leads to an increase in its resonance frequency f_0. The effect mainly depends on the size of a conductive material, as well as on the distance between it and the conducting circuit of the coil [6]. Thus, based on this phenomenon, it becomes possible to tune RF coil to the higher frequency range. The described technique is known as RF shielding. It is a simple method for tuning RF coil compared to the engineering modification of its electric circuit, that can be difficult if MRI user does not have corresponding experience and is undesirable in case of branded coil because of warranty violation.

The application of RF shielding was demonstrated in some works mainly for tuning volume (birdcage) RF coils. In all of them, copper was used as a shield because it is highly conductive (5.8×10^7 S/m) and can be easily formed, fabricated and soldered [7]. In [8], the authors theoretically showed that the presence of a conductive shield reduces the inductance of the resonant system and hence increases the resonance frequency of the birdcage coil. In [9], the same authors developed a technique to change the resonance frequency of a birdcage coil from ^{19}F resonance to ^{1}H resonance by inserting a shield made from one-sided copper polyester and able to be slid in. The authors of [10] implemented mechanical tuning of a ^{1}H birdcage coil using an adjustable RF shield constructed from copper foil tape. Analytical consideration of effects of mutual inductance and shielding in birdcage coils was described in a number of works [11–14].

* Corresponding author.
E-mail addresses: gulyaev@physics.msu.ru (M.V. Gulyaev), ofleurp@mail.ru (O.S. Pavlova), anisimovnv@mail.ru (N.V. Anisimov).

https://doi.org/10.1016/j.jmr.2019.106626
1090-7807/

We know only one full work in which RF shielding technique was applied to a surface RF coil [15]. In that paper, the optimal distance between the copper shield and the conducting circuit of the surface coil (rectangular loop) was determined in order to reduce radiation losses and thereby increase the quality factor *Q*. Another conclusion made by the authors was that when a shield is placed too close to the surface coil, its resonance frequency increases drastically, but the following disadvantages are present: a decrease in quality factor *Q* and the deterioration of the B_1^+ field caused by the near-zone magnetic field compression. The last problem is most relevant, since it leads to a noticeable signal loss in the MR images.

In this paper, we developed the idea of using RF shielding for tuning the resonance frequency of surface coils. We determined how much it is possible to increase the resonance frequency of surface coils by placing a copper shield of different thickness and size directly on the conducting circuit of coils, and showed how to circumvent the problem of a signal loss in the MR images caused by the influence of a copper shield. We tested the proposed method *in vivo* in multinuclear MRI and MRS applications using the shielded surface wired coils and wireless multi-turn multi-gap transmission line resonator (MTMG-TLR). MTMG-TLR serve as a wireless stripline high frequency resonator or self-resonant transceiver, consisting of the concentric RF coils at the opposite sides of a dielectric sheet [16,17]. Thus, the MTMG-TLRs represent a monolithic structure that does not provide for their frequency tuning, unlike other designs of wireless coils. For example, wireless coils can be made of conventional RF circuits consisting of capacitors and inductors [18–20], which can be replaced by simple soldering if the resonance frequency of the coil is incorrect. Another construction is a metamaterial-based system where the frequency of the coil is tuned by changing the length of the brass wires, as they are telescopic [21], or using flexible metasurfaces [22]. In this regard, the interest of using the proposed tuning method for MTMG-TLRs is quite large.

2. Theoretical derivations

The effect of a shield on the resonance frequency and the *Q* value of the coil was described earlier, for example, in [23]. There, two inductively coupled circuits, containing inductances L_c, L_s and resistances R_c, R_s are considered, where the subscript *c* refers to the coil and *s* refers to the shield. Taking into account the effect of mutual induction between the circuits, the effective inductance L_{eff} of the coil will decrease by the value of M^2/L_s, where *M* is the mutual inductance between the coil and the shield. In this case, the resonance frequency f_0 of the coil will be calculated using the formula (1), where *C* is a capacitance of the coil:

$$f_0 = \frac{1}{2\pi\sqrt{\left(L_{c-}\frac{M^2}{L_s}\right)C}} \quad (1)$$

The *Q* value of the coil can be calculated from the formula (2), where $\omega = 2\pi f_0$ is the circular resonance frequency:

$$Q = \frac{\omega\left[L_c - \frac{\omega^2 M^2 L_s}{R_s^2+\omega^2 L_s^2}\right]}{R_c + \frac{\omega^2 M^2 R_s}{R_s^2+\omega^2 L_s^2}} \quad (2)$$

Thus, if the mutual inductance *M* increases, the resonance frequency f_0 of the coil increases and the *Q* value of the coil decreases.

3. Material and methods

The experimental work was performed on a 7.05 T Bruker BioSpec 70/30 USR MR scanner driven by a ParaVision® 5.0 console and equipped with a 105 mT/m gradient amplitude device.

Bruker surface transceivers T6614 and T6615, built on a dual-circuit dual-channel scheme were used to evaluate the effect of a shield on their technical characteristics. The conducting circuit of these coils consists of two flat circular loops with a diameter of 30 mm, separated by a dielectric layer. The mean diameter of the loops is 25 mm. T6614 coil can operate on the Larmor frequency of ^{13}C (75 MHz) and ^{1}H (300 MHz), and T6615 coil – on the Larmor frequency of ^{31}P (121 MHz) and ^{1}H (300 MHz). Further, in the text, if T6614 coil is operating on the frequency of ^{13}C, we will call it as the ^{13}C coil. If T6615 coil is operating on the frequency of ^{31}P or ^{1}H, we will call it as the ^{31}P coil or the ^{1}H coil, respectively. In addition, to implement the planned experiments, the ^{13}C coil was slightly modified. Two electronic components (capacitor of $C \approx 8.2$ pF and inductor of $L \approx 255$ nH) were connected to its electric circuit using the key. As a result, it became possible to change its resonance frequency from ^{13}C to ^{23}Na. Further, in the text, if the ^{13}C coil is operating on the frequency of ^{23}Na we will call it as the ^{23}Na coil.

To estimate the effect of RF shielding on the resonance frequency f_0 and the *Q* value of the coils, we placed the copper plates of various thickness (from 75 μm to 1.5 mm) and diameter (from 8 mm to 30 mm) in the center of their conducting circuit and measured the values of f_0 and *Q*. According to the design of the coils, the copper plates were cut from a roll of copper tape in the shape of a circle. In Fig. 1a, the photograph of the ^{13}C coil with the copper plate placed on its conducting circuit is shown.

For this study, two wireless MTMG-TLRs of 307 MHz and 294 MHz were ordered from the company SEPkoRUS (St. Petersburg, Russia). The main technical characteristics of them were as follows: outer diameter: 30 mm; number of turns: 5; number of gaps: 6; width of the conducting circuit: 1 mm; the distance between the turns: 1 mm and 0.96 mm, respectively. As dielectric, the fluoroplastic material Taconic TLY-5-0050 with dielectric permittivity of 2.2 and thickness of 0.125 mm was used. Further, in the text we will call the first MTMG-TLR as WC1. The second MTMG-TLR was used in this study only with copper plate on its conducting circuit to operate on the same resonance frequency (307 MHz) as the WC1. Further, in the text, when the WC2 is mentioned, it is implied that a second MTMG-TLR with a copper plate placed on its conducting circuit is used. In Fig. 1b, the photograph of the WC2 is shown.

The resonance frequency of 307 MHz for wireless coils is explained the fact that it was assumed to use them as strong inductively coupled with the ^{1}H transceiver volume coil (T10334) of 72 mm inner diameter. It is known that for strongly coupled coil system two peaks are observed on the frequency response curve, i.e. two modes corresponding to the currents parallel (co-rotating current mode) and antiparallel (counter-rotating current mode) [3,24]. Furthermore, a high sensitivity and undistorted B_1^+ field distribution will be observed only when a strong inductively coupled coil system is tuned to a co-rotating current mode [20,25]. For this, it is necessary that the resonance frequency of the coils must be higher than the Larmor frequency of ^{1}H (300 MHz). It was experimentally determined that for our coil configuration, the resonance frequency of the coils should be approximately 307 MHz.

The values of f_0 and *Q* of the surface wired coils were measured with the help of the Network Analyzer Rohde & Schwarz ZVH4 1309.6800.24. The Network Analyzer was also applied for measurement the resonance frequency of the MTMG-TLRs using the single-loop probe method [26].

Phantom measurements were carried out to estimate the degree of a signal loss in the MR images caused by the copper plate. We conducted these studies using the ^{1}H coil with the copper plates on its conducting circuit by changing their diameter and thickness at constant thickness and diameter, respectively. As a phantom, we used a parallelepiped tube made of Plexiglas® with internal dimensions of 24 × 34 × 70 mm filled with water. ^{1}H MR

Fig. 1. ^{13}C coil (a) and MTMG-TLR (b) with a copper plate placed in the center of their conducting circuit.

images of phantom were obtained in the sagittal projection using 2D FLASH method with the following scan parameters: TR/TE = 150/6.0 ms; number of slices: 1; slice thickness: 1 mm; in-plane resolution: 385 × 385 μm; total acquisition time (*TA*): 1 min 18 s; *FA* = 25°. The excited slice was set strictly in the center of the phantom where the maximum signal loss is observed. Then on each of the MR images, the signal attenuation depth was measured using the program ImageJ [27].

In vivo measurements were carried out to obtain multinuclear MR images and spectra using the shielded coils and the Bruker routine coils, and then to compare them. For this purpose, we obtained ^{23}Na MR images and ^{31}P MR spectra of the brain of intact adult male Wistar rat weighing ≈270 g using the ^{23}Na coil, ^{31}P coil and the ^{13}C coil with the copper plates on its conducting circuit. ^{23}Na MR images were acquired using 2D FLASH method with the following scanning parameters: *TR*/*TE* = 10/3.2 ms; no slice selection, in-plane resolution: 0.75 × 0.75 mm^2; *TA* = 1 h 8 min and 16 s; *FA* = 40° that corresponds to the calculated Ernst angle according to ^{23}Na T_1 relaxation time of white and gray matter [28,29]. ^{31}P MR spectra were obtained using 90° pulses of 30 μs duration; number of averages (*NA*) = 4096; *TA* = 26 min 30 s.

In vivo ^{1}H MRI studies were carried out on the brain of intact adult female BALB/c mouse weighing ≈35 g using the strong inductively coupled coil systems consisting of the ^{1}H transceiver volume coil and the WC1 or WC2. To acquire T_1-weighted ^{1}H MR images of the mouse brain, 2D FLASH method was used with the following scanning parameters: *TR*/*TE* = 270/5.5 ms; in-plane resolution: 0.13 × 0.13 mm^2; 10 slices with slice thickness of 1 mm; *TA* = 3 min and 30 s; *FA* = 25°. For MR angiography, 3D FLASH pulse sequence was applied with the following acquisition parameters: *TR*/*TE* = 12.8/4.1 ms, *FA* = 20°; in-plane resolution: 0.13 × 0.13 × 0.13 mm^3; *TA* = 10 min 30 s. Processing of the acquired MR images was performed using the program ImageJ.

In vivo studies were conducted in accordance with the European Community Council directives 86/609/EEC, and the local institutional animal ethics committee approved the study. During the MRI studies, the animals were anesthetized with the mixture of isoflurane and oxygen.

4. Experimental results and discussion

4.1. Phantom measurements

We estimated the shift of the resonance frequency f_0 and the decrease in the loaded *Q* value of the surface wired coils when the copper plates of different diameter were placed on their conducting circuit. For this, the copper plates of 75 μm thickness were used. In Fig. 2 the dependency graphs of the resonance frequency f_0 and the loaded *Q* value of the coils on the parameter *d*/*D* are presented, where *d* is the external diameter of the copper plate and *D* – the mean diameter of the conducting circuit of the coils.

As the measurements have shown, the resonance frequency f_0 of the coils increases with increasing the diameter of the copper plate, but the dependence is nonlinear. The dependence in Fig. 2a corresponds to the formula (1) until the diameter *d* of the copper plate is less than the mean diameter *D* of the conducting circuit of the coils. If *d* > *D* the dependence is changed and the resonance frequency f_0 tends to the constant value. This may be due to the fact that, when *d* > *D*, the effective capacitance between the

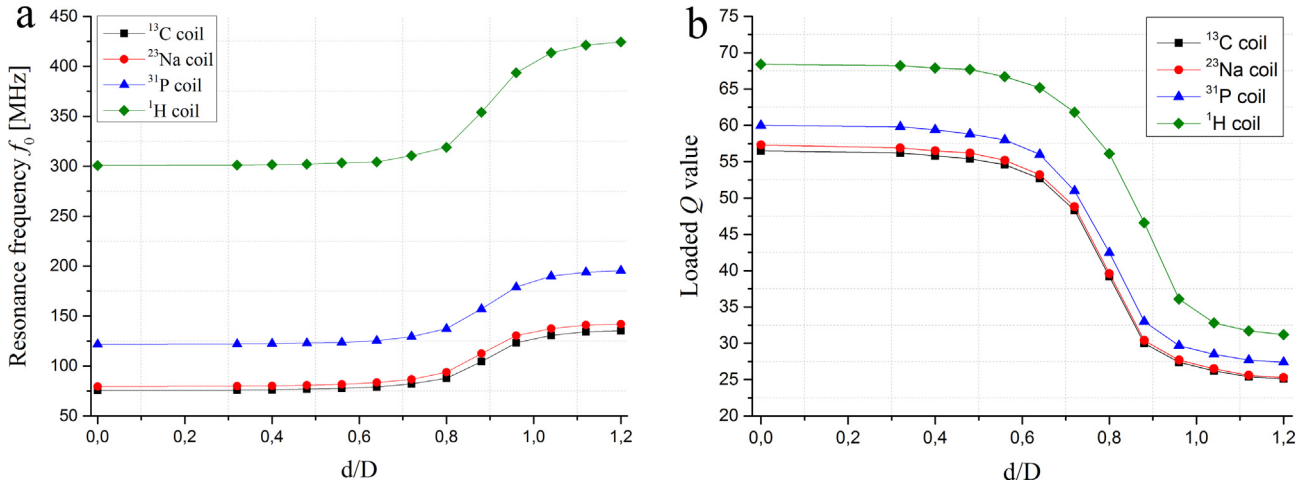

Fig. 2. The dependency graphs of the resonance frequency f_0 (a) and the loaded *Q* value (b) of the ^{13}C coil, ^{23}Na coil, ^{31}P coil and ^{1}H coil on the parameter *d*/*D*, where *d* is the external diameter of the copper plate and *D* – the mean diameter of the conducting circuit of the coils. The thickness of copper plates is ≈75 μm. The coils were loaded with a phantoms filled with ^{13}C glucose solution, the saturated NaCl solution, 85% H_3PO_4 solution and H_2O, respectively.

conducting circuit and the copper plate increases drastically – the more d, the more the capacitance. Probably, the increase in the effective capacitance is compensated by the decrease in the effective inductance of the coil and the resonance frequency f_0 no longer has a perceptible growth. The maximum relative increase in the resonance frequency f_0 due to the use of the copper plates reaches ≈80% for the ^{13}C coil and ^{23}Na coil, ≈60% for the ^{31}P coil and ≈35% for the ^{1}H coil.

As seen from Fig. 2b, the loaded Q values for all tested coils decrease with increasing the diameter of the copper plate and the greatest decline is observed when the copper plate overlaps the conducting circuit of the coils. In this case, the mutual inductance M and the resonance frequency f_0 significantly increase, which leads to a perceptible growth of the denominator in the formula (2). If $d > D$ the dependence changes, and the loaded Q value tends to the constant value, since the values of f_0 and M no longer greatly increase.

According to the graphs in Fig. 2, it is possible to compare the efficiency of using a copper plate for tuning the resonance frequency of the surface coil. In particular, the use of the copper plate with a diameter of 17 mm (d/D = 0.68) leads to retuning the ^{13}C coil from 75 MHz to 79 MHz (the Larmor frequency of ^{23}Na in 7.05 T). In this case, the loaded Q value slightly decreases from 56 to 48. In turn, the use of the copper plate with a diameter of 24 mm (d/D = 0.96) leads to retuning the ^{13}C coil from 75 MHz to 121 MHz (the Larmor frequency of ^{31}P in 7.05 T). However, at the same time, the significantly decrease in its loaded Q value from 56 to 28 is observed. These values of Q are less than those that can be obtained for the Bruker routine ^{23}Na and ^{31}P coils, in 1.3 and 2.5 times, respectively. This will undoubtedly affect the decrease in the signal-to-noise ratio (SNR) in the MR images and spectra, but most importantly is that the loaded Q values of the coils do not fall to zero if the copper plates are applied.

We have also estimated how the thickness of the cooper plate influences on the technical characteristics of the surface coil. We carried out these measurements for the ^{1}H coil with the copper plates of different diameter: 16 mm, 22 mm and 26 mm which corresponds to different values of the parameter d/D: 0.64, 0.88 and 1.04, respectively. To increase the thickness of the copper plate, we stuck one plate to another strictly in the center of the conducting circuit of the ^{1}H coil. The initial thickness of the plates was 75 μm. In Fig. 3, the dependency graphs of the resonance frequency f_0 and the Q value of the ^{1}H coil on the thickness of the copper plates are presented.

Fig. 3 shows that the thickness of the copper plate does not have a significant effect on the resonance frequency f_0 and the loaded Q value of the surface coil, and no matter what the diameter of the plate is used.

As it was mentioned in the Section 3 Material and methods, the degree of a signal loss in the MR images we estimated using the ^{1}H coil with the copper plates on its conducting circuit by changing their diameter at constant thickness (first type of dependency) and by varying their thickness at constant diameter (second type of dependency). Since the resonance frequency f_0 and the loaded Q value of the surface coil are practically independent on the thickness of the plate (see Fig. 3), to determine the first type of dependency we used the plates of 75 μm thickness – the minimal thickness of the copper foil we had. Since, the resonance frequency of the surface coil increases with increasing the diameter of the copper plate, it is possible to determine the second type of dependency only for plates which do not have an observable effect on the frequency. Considering this fact, we chose the plates of d < 0.64D.

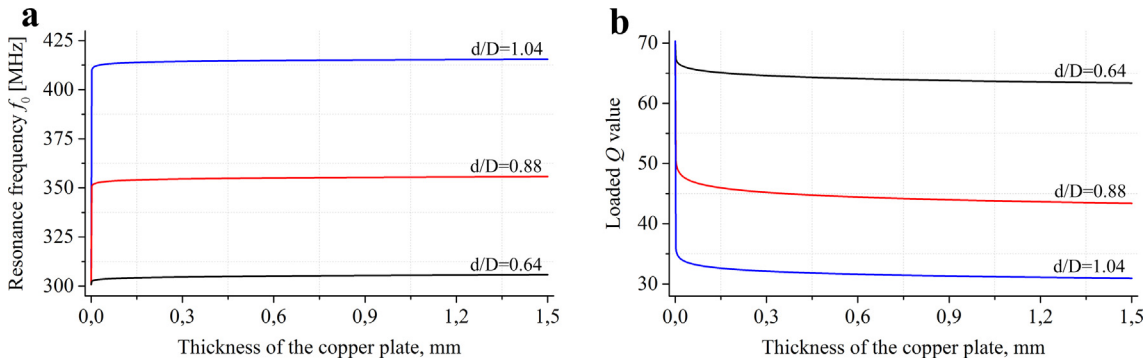

Fig. 3. The dependency graphs of the resonance frequency f_0 and the loaded Q value of the ^{1}H coil on the thickness of the copper plates placed on its conducting circuit. The graphs were plotted for different diameter of the copper plates: 16 mm, 22 mm and 26 mm which corresponds to different values of the parameter d/D: 0.64, 0.88 and 1.04, respectively. The ^{1}H coil was loaded with a phantom filled with H_2O.

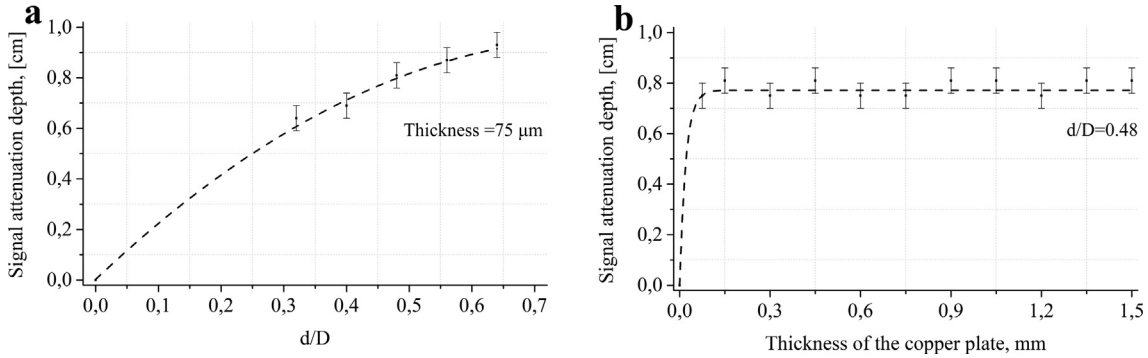

Fig. 4. The dependency graphs of the signal attenuation depth on the parameter d/D (a) and on the thickness of the copper plate placed on the conducting circuit of the ^{1}H coil (b).

In this case, the resonance frequency of the ^{1}H coil arises by only few MHz, which makes it possible to tune its resonance frequency to the Larmor frequency of ^{1}H using the nominal variable inductance. The results of these measurements are presented in Fig. 4.

Fig. 4a shows that with increase in the diameter of the copper plate, the signal attenuation depth also increases. Thus, when using the copper plate of $d \approx D$, in addition to the low Q value, the signal will have a greater attenuation depth in the MR image. These two

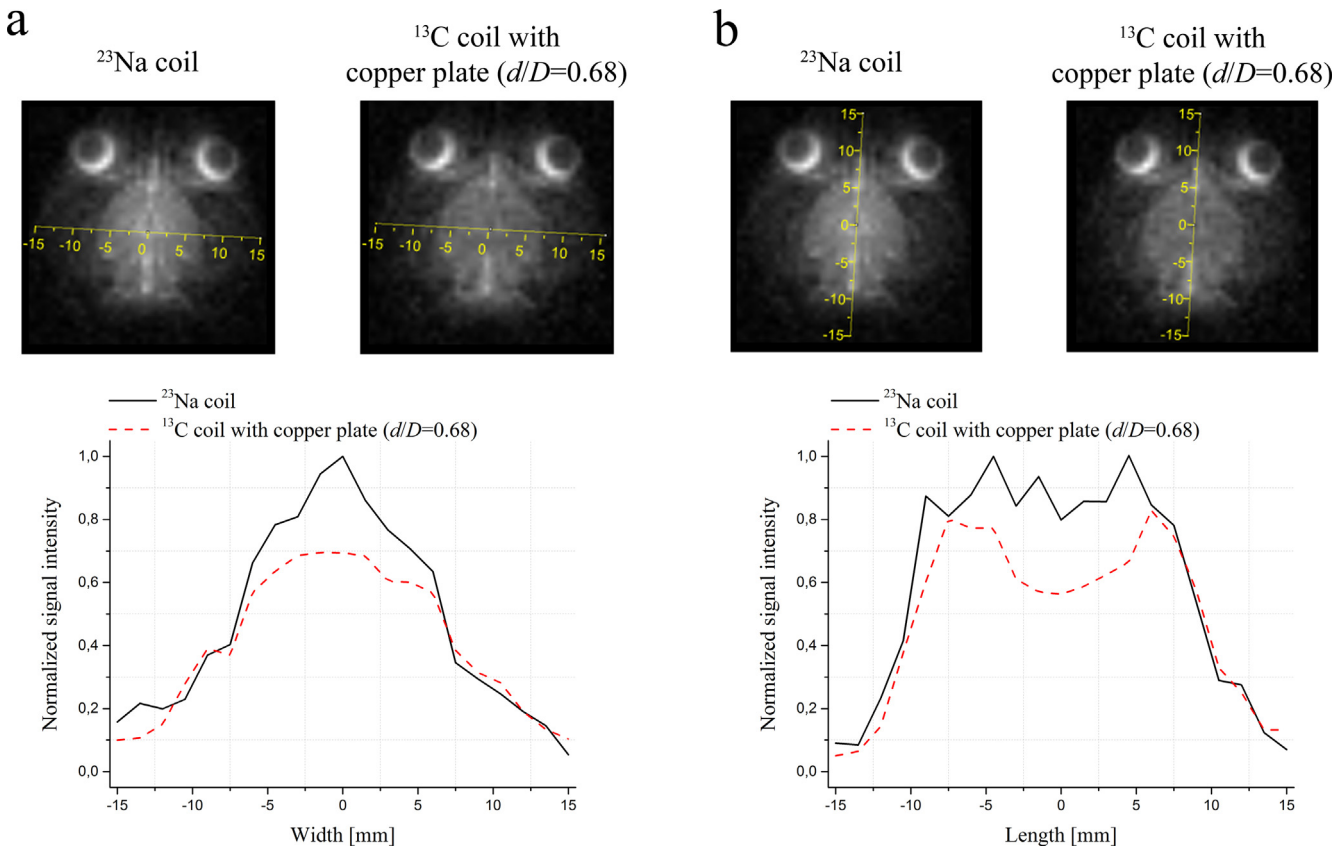

Fig. 5. Coronal ^{23}Na MR images of the rat brain and ^{23}Na MR signal intensity profiles obtained using the ^{23}Na coil and the ^{13}C coil with the copper plate of 17 mm diameter (d/D = 0.68), plotted through the center of the brain in the left-right (a) and anterior-posterior (b) directions.

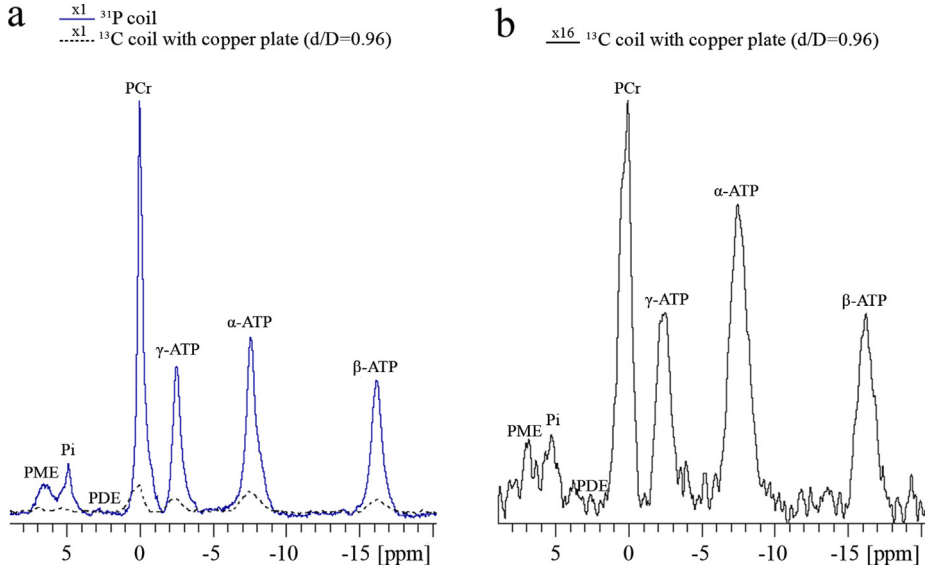

Fig. 6. Rat brain ^{31}P MR spectra acquired using the ^{31}P coil (a, blue line spectrum) and the ^{13}C coil with the copper plate of 24 mm diameter (d/D = 0.96) (a, black dash spectrum). (b) 16 times enlarged view of the ^{31}P MR spectrum acquired using the ^{13}C coil with the copper plate of 24 mm diameter (d/D = 0.96). PCr – phosphocreatine. α-ATP, β-ATP, γ-ATP – adenosine Triphosphate. Pi – inorganic phosphate. PME – phosphomonoester. PDE – phosphodiester.

factors can greatly affect the quality of the MR images and spectra. At the same time, in Fig. 4b it is shown that the thickness of the copper plate does not have a significant effect on the signal attenuation depth. For this reason, in *in vivo* measurements, we used the copper plates of 75 μm thickness.

4.2. In vivo measurements

^{23}Na MR images were obtained using the ^{23}Na coil and then using the ^{13}C coil with the copper plate of 17 mm diameter (d/D = 0.68). In Fig. 5, the corresponding rat brain coronal ^{23}Na MR images are shown. Under the images, the profiles of the MR signal intensity normalized to the maximum signal intensity are presented. The profiles were plotted through the center of the rat brain in the left-right (Fig. 5a) and anterior-posterior (Fig. 5b) directions. Black line curves correspond to the signal intensity profiles obtained using the ^{23}Na coil, and red dash curves correspond to the signal intensity profiles obtained using the ^{13}C coil with the copper plate of 17 mm diameter (d/D = 0.68).

As follows from Fig. 5, in the brain region covered by the copper plate, the MR signal intensity is lower than in the case of using the unshielded ^{23}Na coil. This makes it difficult to visualize the ventricles of the brain. The maximum decline of the signal intensity in this region equals to ≈ 31% and ≈39% in the left-right and anterior-posterior directions, respectively. At the same time, at the level of the eye orbits and the cerebellum, i.e. in the region where the effect of the copper plate is minimum, the MR signal intensities are the same.

We also performed ^{31}P MRS studies using the ^{31}P coil and then using the ^{13}C coil with the copper plate of 24 mm diameter (d/D = 0.96). In Fig. 6, the corresponding rat brain ^{31}P MR spectra are shown.

Note that the ^{31}P MR spectrum acquired using the ^{13}C coil with the copper plate of 24 mm diameter (d/D = 0.96) is characterized by 16 times lower signal amplitude and lines broadening in comparison with using the unshielded ^{31}P coil. The line broadening is caused by the deterioration of the B_1^+ field, and the decrease in signal amplitude mainly due to the low Q value. Thus, the

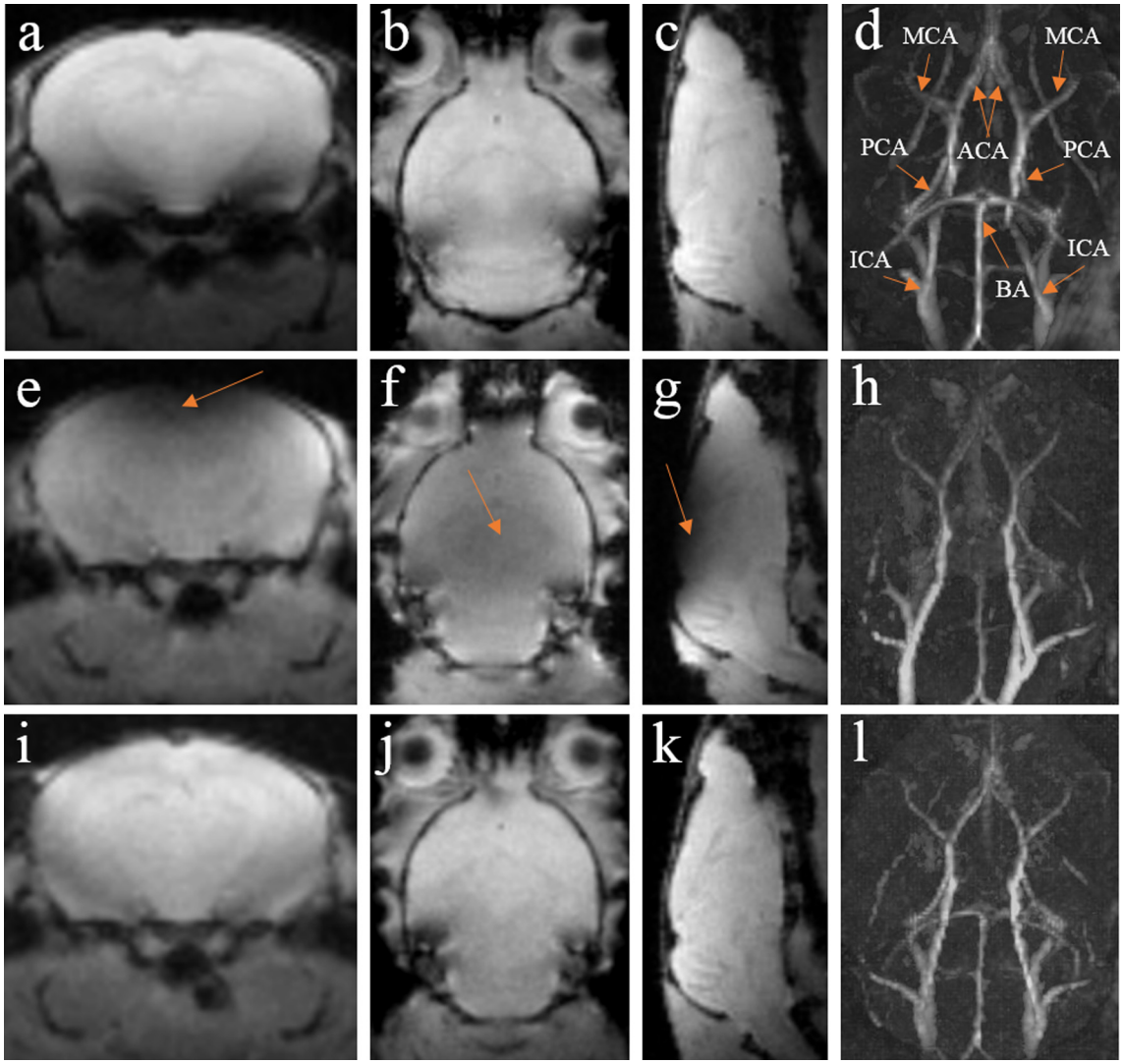

Fig. 7. Mouse brain T_1 weighted ^{1}H MR images in the axial (a, e, i), coronal (b, f, j) and sagittal (c, g, k) projections and MR angiograms (d, h, l) obtained using the Bruker T10334 coil together with the WC1 (upper row) and together with the WC2 (middle and lower row). Upper row: the WC1 is placed extremely close to the mouse head. Middle row: the WC2 is placed extremely close to the mouse head. Lower row: the WC2 is placed at the distance of ≈4 mm from the mouse head. Arrows in the middle row point to the regions of the signal loss caused by the copper plate. BA – basilar artery. ICA – internal carotid arteries. ACA – anterior cerebral arteries. MCA – middle cerebral arteries. PCA – posterior cerebral arteries.

measurements showed that, for example, the linewidth (width at half height) for phosphocreatine (PCr) signal equals to 115 Hz when using the ^{13}C coil with the copper plate vs 46 Hz when using the unshielded ^{31}P coil. Nevertheless, in the both ^{31}P MR spectra, seven major metabolite signals are well resolved. Among them are: PCr at 0 ppm, three peaks of Adenosine Triphosphate (α-ATP, β-ATP, γ-ATP), seen at −7.7, −16.3 and −2.7 ppm, Phosphodiester (PDE) at 2.6 ppm, Inorganic Phosphate (Pi) at 4.9 ppm and Phosphomonoester (PME) at 6.3 ppm [30].

Before conducting ^{1}H MRI studies, we first determined that the copper plate of 13 mm diameter should be placed on the conducting circuit of the second MTMG-TLR to increase its resonance frequency from 294 MHz to 307 MHz. Then, we obtained the series of mouse brain ^{1}H MR images and MR angiograms using Bruker T10334 coil together with the WC1 and then together with the WC2 (Fig. 7).

As seen from Fig. 7 (upper row), in the case of using the Bruker T10334 coil together with the WC1, ^{1}H MR images and MR angiograms are of good quality and the main vessels are well observed. Among them are: BA – basilar artery, ICA – internal carotid arteries, ACA – anterior cerebral arteries, MCA – middle cerebral arteries, PCA – posterior cerebral arteries [31].

When using the Bruker T10334 coil together with the WC2, the signal loss is observed in the region of influence of the copper plate. This is inherent for the both ^{1}H MR images and MR angiograms – Fig. 7 (middle row). Thus, for example, the visualization of the brain and main vessels is deteriorated, but the areas outside the copper plate location, such as olfactory bulb and cerebellum, are clearly visible. We measured the signal attenuation depth in the sagittal MR image of the brain. It was equal ≈4 mm. This means that the magnetic field compression zone corresponds to the same ≈4 mm, and at a distance of ≈4 mm and more from the copper plate location, the B_1^+ field has a typical shape created by any surface coil. Therefore, if the WC2 is placed at the distance of ≈4 mm and more from the mouse head, the obtained MR images will be without the signal loss. On the other hand, in the case of using a surface coil, the maximum *SNR* values in MR images can be obtained when the coil is located extremely close to the region of interest. With increasing the distance between the coil and the region of interest, the *SNR* values decrease. With this in mind, in order to achieve acceptable *SNR* values without a signal loss in the MR images we suggest placing the shielded surface coil from the region of interest at a distance equal to the measured signal attenuation depth. In Fig. 7 (lower row), ^{1}H MR images and MR angiograms were obtained when the WC2 was placed at the distance of ≈4 mm from the mouse head. As can be noted, a signal loss is not visible and the diagnostic informativeness is save.

In Fig. 8, we combined the results of *in vivo* ^{1}H MRI studies. It presents the mouse brain sagittal ^{1}H MR images and the corresponding signal intensity profiles obtained for three above mentioned cases. The signal intensity profiles are plotted along lines drawn in ^{1}H MR images and parallel to length and width axes. The horizontal and vertical lines are drawn perpendicularly and parallel to the planes of the wireless coils, respectively.

Black line curves in Fig. 8d and 8e represent the normalized MR signal intensity profiles in ^{1}H MR images obtained using Bruker T10334 coil together with the WC1 (Fig. 8a). It can be seen that the signal decreases with the distance from the plane of the WC1

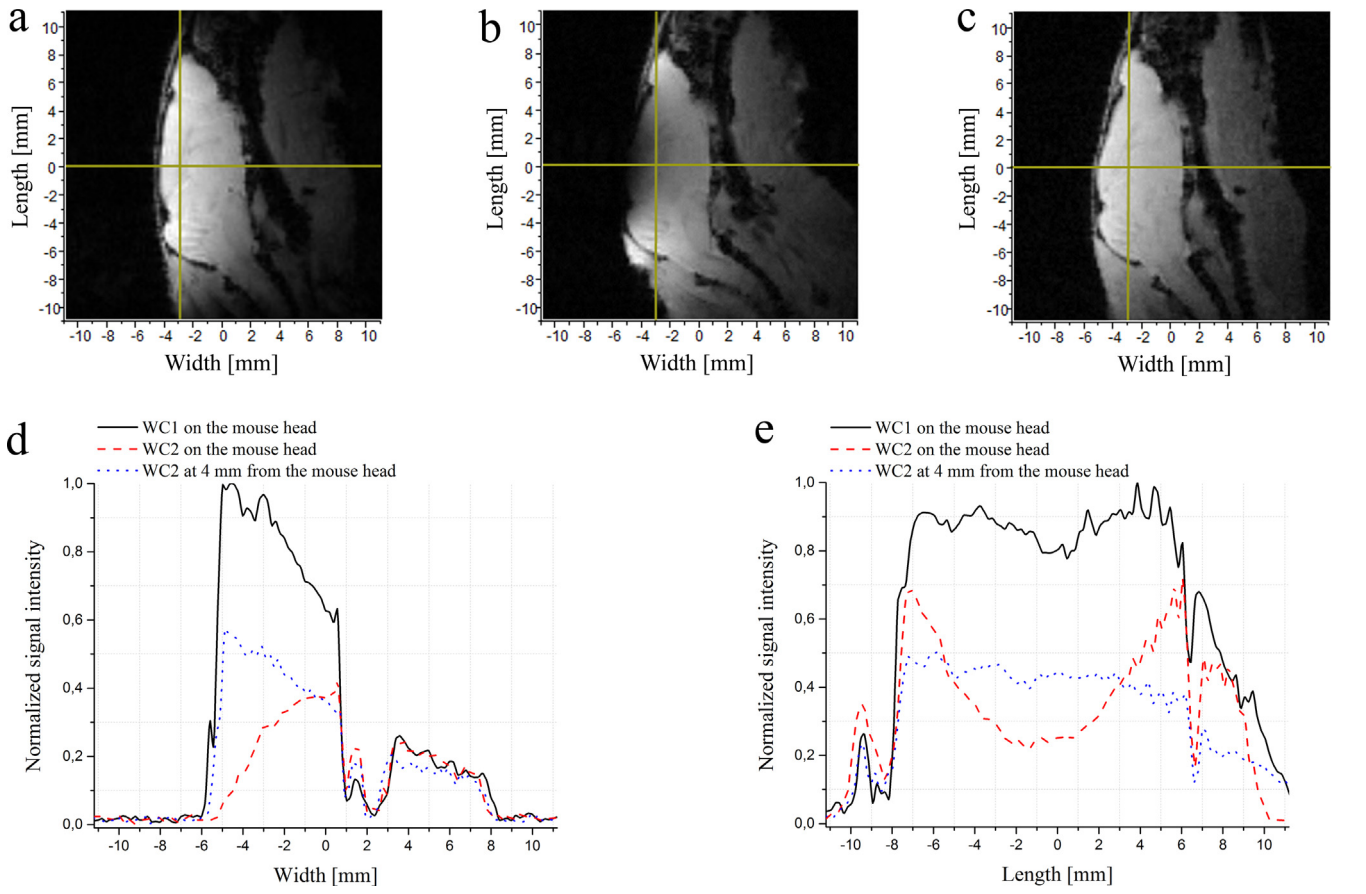

Fig. 8. Mouse brain sagittal ^{1}H MR images and the corresponding signal intensity profiles obtained using Bruker T10334 coil together with the WC1 (a) and together with the WC2 (b, c). In (a, b) the wireless coils are placed extremely close to the mouse head. In (c) the WC2 is placed at the distance of ≈4 mm from the mouse head (c). Signal intensity profiles are plotted along horizontal (d) and vertical (e) lines drawn in ^{1}H MR images.

(Fig. 8d) and it is homogeneous in anterior-posterior direction (Fig. 8e).

When Bruker T10334 coil together with the WC2 are used (Fig. 8b), the signal drops only in the region of influence of the copper plate. The signal intensity profiles for this case are shown as red dash curves in Fig. 8d and 8e. The signal loss occurs in the central region of the profiles (-5 mm <–> -1 mm in Fig. 8d, -7 mm <–> 6 mm in Fig. 8e). Thus, the depth of the signal loss is ≈4 mm and the width of the signal loss corresponds to the diameter of the copper plate ($d = 13$ mm). In the left-right direction, from 2 mm the signal is completely aligned with black line curve. In the anterior-posterior direction, the edge values (<-7 mm and >6 mm) of the signal intensity are aligned with black line curve too.

Blue dot curves represent the normalized MR signal intensity profiles that were obtained when the WC2 is placed at the distance of ≈4 mm from the mouse head (Fig. 8c). Corresponding profiles coincide qualitatively with profiles obtained using the WC1 placed extremely close to the mouse head, however the normalized MR signal intensity is 2–3 times lower. This signal reduction is not significant, but if you want, you can fix this problem by increasing the number of signal averages.

5. Conclusion

The use of RF shield placed on the conducting circuit of the surface coils provides additional options for tuning the resonance frequency of the coils to the higher frequency range. This is a very simple and technically easy method for implementation. However, the main disadvantage of the method is the signal loss in MR images and line broadening in MR spectra.

To circumvent this problem it is suggested to place the shielded RF surface coil, whether wired or wireless, at some distance from the region of interest. This distance should corresponds to the signal attenuation depth, which can be measured when the shielded coil is placed extremely close to the object. To fix the problem of decreasing *SNR* values in MR images and spectra, as well as low *Q* values of the shielded coils, you should increase the number of signal averages.

Acknowledgements

This study was carried out at the Moscow State University on the equipment of the Collective Using Center «Biospectrotomography» and supported by Russian Science Foundation Grant no. 17-79-10448.

References

[1] J.T. Vaughan, J.R. Griffiths, RF Coils for MRI, John Wiley & Sons Ltd, Chichester, West Sussex, 2012.
[2] P.A. Bottomley, J.R. Griffiths, Handbook of Magnetic Resonance Spectroscopy In Vivo. MRS Theory, Practice and Applications, John Wiley & Sons Ltd, Chichester, 2016.
[3] P.J. Cassidy, K. Clarke, D.J. Edwards, Determining the tuning and matching requirements of RF coils using electromagnetic simulation and electric circuit analysis, Concepts Magn. Reson. Part B 25B (1) (2005) 27–41.
[4] L. Tugan Muftuler, G. Gulsen, K.D. Sezen, O. Nalcioglu, Automatic tuned MRI RF Coil for multinuclear imaging of small animals at 3T, J. Magn. Reson. 155 (1) (2002) 39–44.
[5] R.L. Myers, The Basics of Physics, Greenwood, Westport, Conn, 2006.
[6] J. Jin, Electromagnetic Analysis and Design in Magnetic Resonance Imaging, CRC, Boca Raton, FL, 1999.
[7] W.H. Hayt Jr., J.A. Buck, Engineering Electromagnetics, sixth ed., McGraw-Hill, 2001.
[8] P.M. Joseph, D. Lu, A technique of double resonant operation of birdcage imaging coils, IEEE Trans. Med. Imaging 8 (3) (1989) 286–294.
[9] D.F. Lu, P.M. Joseph, A technique of double-resonant operation of 19F and 1H quadrature birdcage coils, Magn. Reson. Med. 19 (1) (1991) 180–185.
[10] B.J. Dardzinski, S. Li, C.M. Collins, G.D. Williams, M.B. Smith, A birdcage coil tuned by RF shielding for application at 9.4 T, J. Magn. Reson. 131 (1) (1998) 32–38.
[11] R. Pascone, T. Vullo, J. Farelly, P.T. Cahill, Explicit treatment of mutual inductance in eight-column birdcage resonators, Magn. Reson. Imaging 10 (3) (1992) 401–410.
[12] J. Jin, G. Shen, T. Perkins, A simple method to incorporate the effects of an RF shield into RF resonator analysis for MRI applications, IEEE Trans. Biomed. Eng. 42 (8) (1995) 840–843.
[13] C.M. Collins, S. Li, Q.X. Yang, M.B. Smith, A method for accurate calculation of B1 fields in three dimensions: effects of shield geometry on field strength and homogeneity in the birdcage coil, J. Magn. Reson. 125 (2) (1997) 233–241.
[14] S. Crozier, L.K. Forbes, W.U. Roffmann, K. Luescher, D.M. Doddrell, Currents and fields in shielded RF resonators for NMR/MRI, Meas. Sci. Technol. 7 (7) (1996) 1083–1086.
[15] K.C. Ong, H. Wen, A.S. Chesnick, S. Duewell, F.A. Jaffer, R.S. Balaban, Radiofrequency shielding of surface coils at 4.0 T, J. Magn. Reson. Imaging 5 (6) (1995) 773–777.
[16] R. Frass-Kriegl, E. Laistler, S. Hosseinnezhadian, A.I. Schmid, E. Moser, M. Poirier-Quinot, L. Darrasse, J.-C. Ginefri, Multi-turn multi-gap transmission line resonators – concept, design and first implementation at 4.7 T and 7 T, J. Magn. Reson. 273 (2016) 65–72.
[17] A. Protopopov, M.V. Gulyaev, O.S. Pavlova, E.A. Mokhova, Yu.A. Pirogov, Computation of the resonance frequencies of the transmission line resonators used in MRI, Magn. Reson. Imaging 61 (2019) 167–174.
[18] X. Silver, W. Xu Ni, E.V. Mercer, B.L. Beck, E.L. Bossart, B. Inglis, T.H. Mareci, In vivo 1H magnetic resonance imaging and spectroscopy of the rat spinal cord using an inductively-coupled chronically implanted RF coil, Magn. Reson. Med. 46 (6) (2001) 1216–1222.
[19] M. Bilgen, Magnetic resonance microscopy of spinal cord in mouse using a miniaturized implantable RF coil, J. Neurosci. Methods 159 (1) (2007) 93–97.
[20] N.A. Volland, T.H. Mareci, I. Constantinidis, N.E. Simpson, Development of an inductively coupled MR coil system for imaging and spectroscopic analysis of an implantable bioartificial construct at 11.1 T, Magn. Reson. Med. 63 (4) (2010) 998–1006.
[21] A. Hurshkainen, A. Nikulin, E. Georget, B. Larrat, D. Berrahou, A.L. Neves, P. Sabouroux, S. Enoch, I. Melchakova, P. Belov, S. Glybovski, R. Abdeddaim, A Novel Metamaterial-Inspired RF-coil for Preclinical Dual-Nuclei MRI, Sci. Rep. 8 (1) (2018) 9190.
[22] R. Schmidt, A. Slobozhanyuk, P. Belov, A. Webb, Flexible and compact hybrid metasurfaces for enhanced ultra high field in vivo magnetic resonance imaging, Sci. Rep. 7 (1) (2017) 1678.
[23] K.L. Kaiser, Electromagnetic shielding, CRC Press, Boca Raton, 2005.
[24] M. Bilgen, Inductively-overcoupled coil design for high resolution magnetic resonance imaging, Biomed. Eng. Online 5 (3) (2006).
[25] M.V. Gulyaev, O.S. Pavlova, D.V. Volkov, N.V. Anisimov, Yu.A. Pirogov, The use of strong inductively coupled wireless surface coil and transmit/receive volume coil for 1H/19F MRI, Appl. Magn. Reson. 50 (1–3) (2018) 403–413.
[26] J.-C. Ginefri, E. Durand, L. Darrasse, Quick measurement of nuclear magnetic resonance coil sensitivity with a single-loop probe, Rev. Sci. Instrum. 70 (12) (1999) 4730–4731.
[27] G. Schneider, W. Rasband, K. Eliceiri, NIH Image to ImageJ: 25 years of image analysis, Nat. Methods 9 (2012) 671–675.
[28] G. Helms, H. Dathe, N. Weiskopf, P. Dechent, Identification of signal bias in the variable flip angle method by linear display of the algebraic Ernst equation, Magn. Reson. Med. 66 (3) (2011) 669–677.
[29] G. Madelin, R.R. Regatte, Biomedical applications of sodium MRI in vivo, J. Magn. Reson. Imaging 38 (3) (2013) 511–529.
[30] N.E.P. Deutz, W.M.M.J. Bovée, R.A.F.M. Chamuleau, Brain 31P NMR spectroscopy in the conscious rat, J. Neurosci. Meth. 16 (2) (1986) 157–161.
[31] G. Pastor, M. Jiménez-González, S. Plaza-García, M. Beraza, D. Padro, P. Ramos-Cabrer, T. Reese, A general protocol of ultra-high resolution MR angiography to image the cerebro-vasculature in 6 different rats strains at high field, J. Neurosci. Meth. 289 (2017) 75–84.